ELSEVIER

Biophysical Chemistry 129 (2007) 43–48

Biophysical Chemistry

http://www.elsevier.com/locate/biophyschem

Spatial distribution of dielectric shielding in the interior of *Pyrococcus furiosus* rubredoxin as sampled in the subnanosecond timeframe by hydrogen exchange

David M. LeMaster [a], Janet S. Anderson [b], Griselda Hernández [a,*]

[a] *Wadsworth Center, New York State Department of Health and Department of Biomedical Sciences, School of Public Health, University at Albany-SUNY, Empire State Plaza, Albany, New York, 12201 USA*

[b] *Department of Chemistry, Union College, Schenectady, New York, 12308 USA*

Received 6 March 2007; received in revised form 8 May 2007; accepted 10 May 2007
Available online 18 May 2007

Abstract

Experimental p*K* values of ionizable sidechains provide the most direct test for models representing dielectric shielding within the interior of a protein. However, only the strongly shifted p*K* values are particularly useful for discriminating among models. NMR titration studies have usually found only one or two such shifted p*K* values in each protein, so that the fitting of the experimental data to a uniform internal dielectric (ε_{int}) model is not well constrained. The observed variation among proteins for such ε_{int} estimates may reflect nonuniformity of dielectric shielding within each protein interior or qualitative differences between individual proteins. The differential amide kinetic acidities for a series of metal-substituted rubredoxins are shown to be consistent with Poisson–Boltzmann predictions of dielectric shielding that is relatively uniform for all of the amides that are sensitive to the metal charge, a region which corresponds to roughly 1/3 of the internal volume. The effective ε_{int} values near 6 that are found in this study are significantly lower than many such estimates derived from sidechain p*K* measurements. The differing timeframes in which dielectric relaxation can respond to the highly transient peptide anion as compared to the longer lived states of the charged sidechains offers an explanation for the lower apparent dielectric constant deduced from these measurements.

Keywords: Protein ionization; Hydrogen exchange; Charged state lifetime; Electrostatics; Dielectric relaxation

1. Introduction

Globular proteins are structurally ordered polyelectrolytes that exhibit complex electrostatic interactions which play a central role in their biological functions in catalysis and signal transduction. Efforts to understand dielectric shielding within the protein interior [1] predate the initial X-ray structure determination of myoglobin [2], and this challenge continues to drive an active field of research [3–5]. Explicit full system ab initio simulation of the electronic and conformational contributions to electrostatic forces arising from the protein chain and the surrounding aqueous phase and solutes remains impractical. Electrostatic modeling on the basis of an effective internal dielectric constant has continued to be fruitful, despite the well-recognized shortcomings inherent in the application of this macroscopic bulk phase parameter to the atomic scale [6]. However, progress beyond a simple internal dielectric constant representation is, in part, impeded by the limited set of experimental data that can serve as significant constraints in the testing of more complex representations of the electrostatic interactions.

The p*K* values of ionizable protein sidechains provide the most readily accessible experimental monitor of local electrostatic interactions. Hundreds of protein sidechain p*K* values have been measured, primarily by NMR titration studies [7]. However, the vast majority are only weakly perturbed from model peptide p*K* values, largely reflecting the efficient shielding by the water molecules that surround solvent-exposed sites. Since such highly hydrated charged sidechains are

* Corresponding author. Tel.: +1 518 474 4673; fax: +1 518 473 2900.
E-mail address: griselda@wadsworth.org (G. Hernández).

0301-4622/$ - see front matter © 2007 Elsevier B.V. All rights reserved.
doi:10.1016/j.bpc.2007.05.004

generally poorly ordered in X-ray or NMR structural analyses, reliable modeling of their electrostatic interactions is often problematic. Indeed for most cases, the assumption that the protein sidechain p*K* values are not perturbed from their simple peptide reference values provides predictions of the experimental p*K* values as accurately as does conventional Poisson–Boltzmann modeling [8].

Reliable discrimination among various approaches to modeling protein electrostatic interactions requires a focus on those sidechain p*K* values that are substantially shifted from their peptide reference values [6]. Unfortunately, the modest-sized proteins for which the NMR titrations are well-characterized rarely have more than one or two ionizable sidechains possessing strongly shifted p*K* values that are sensitive to the dielectric shielding of the protein interior. Poisson–Boltzmann style analyses of individual proteins containing such strongly shifted p*K* values have predicted a wide range of values for the internal dielectric [9–13]. Applying an identical electrostatic analysis to 7 different proteins for structurally buried sidechains having p*K* values shifted by at least 2 units yielded ε_{int} values ranging from 10 to 23 [11,14]. Still unclear is the degree to which such differing ε_{int} values for these ionizable sidechains indicate differences in the average dielectric shielding for the various proteins, or rather the presence of nonuniformity in the dielectric interactions across the interior of each individual protein. However, with the use of a larger set of backbone amide p*K* values that simultaneously monitor the internal dielectric response of a given protein, the standard Poisson–Boltzmann calculations can offer insight into this problem. With the effective internal dielectric viewed primarily as an adjustable parameter, the existence of substantial spatial heterogeneity in the dielectric shielding within an individual protein should be reflected in the range of predicted ε_{int} values.

2. Materials and methods

Hydrogen atoms were added to the X-ray coordinates of *Pf* rubredoxin (pdb code 1BQ8 [15]) with the program Reduce [16]. Nonlinear Poisson–Boltzmann calculations were carried out using the DelPhi algorithm [17]. PARSE partial charges and ionic radii [18] were used for all protein atoms except C^{β} and S^{γ} of the cysteine residues. Partial charges for these atoms and for the Zn(II) and Ga(III) atoms were taken from quantum mechanical calculations on the Fe(II)- and Fe(III)-containing tetramethylthiolate complex [19,20]. The metal site geometries of the Zn(II)- [21] and Fe(II)- [22] substituted rubredoxins as well as the Ga(III)- [23] and Fe(III)- [24] substituted rubredoxins are known to be essentially indistinguishable in the X-ray analyses at near 1 Å resolution. Ionic radii of 0.7 Å and 0.6 Å were used for Zn(II) and Ga(III), respectively. The 1.1 Å resolution structure of *Pf* rubredoxin does not contain any internal cavities large enough to contain a water molecule [25] for potential inclusion in the Poisson–Boltzmann calculations. The grid size was 167 with a 50% filling factor. The external dielectric was set to 80.0, the salt concentration to 0.10 M, and the ionic radius to 2.0. The protein sample of the 1BQ8 X-ray structure contains an N-terminal Met-Ala sequence, while the NMR analysis was carried on a variant containing an N-terminal Met-Lys sequence [26].

3. Results and discussion

3.1. Dielectric shielding in Pf rubredoxin amide exchange

Recently we [27] reported that the individual residue base-catalyzed amide hydrogen exchange rates of *Pyrococcus furiosus* (*Pf*) rubredoxin vary by up to a million-fold when the metal binding site is substituted with the isoelectronic series of Zn(II), Ga(III) and Ge(IV). The amides considered in this analysis exhibit denaturant concentration-independent exchange rates under these conditions [28], consistent with exchange via local conformational fluctuations. If these differential exchange rates arise from metal charge-dependent changes in the free energies of the conformational transitions required to enable the hydrogen exchange reaction, ΔG variations of up to more than 8 kcal/mol would be required. However, independent experimental estimate of the differential conformational stability for the metal charge states of the rubredoxins is at most 1 kcal/mol [29].

A direct electrostatic basis for these differential exchange rates is indicated by the fact that the log ratio of the rate constants vary inversely with distance out to at least 12 Å from the metal site (Fig. 1), consistent with a simple Coulomb's Law dependence in a uniform dielectric. This region of the protein structure corresponds to the so-called rubredoxin knuckle, common to nearly all members of the zinc finger superfamily [30]. The tetrathiolate coordination yields a Zn(II) metal cluster carrying a net charge of–2. The resultant electrostatic potential serves to destabilize the peptide anion transition state that is formed when the amide proton is removed by hydroxide ion. Substitution with Ge(IV) yields a neutral metal cluster and a corresponding acceleration of the base-catalyzed hydrogen exchange rates.

To provide a more realistic representation of the electrostatic interactions, Poisson–Boltzmann calculations were carried out to predict the electrostatic potential at each backbone nitrogen in *Pf* rubredoxin on the basis of an external solvent phase with a dielectric constant of 80 and an adjustable uniform dielectric for the protein volume. The metal charge-dependent variation in the local electrostatic potential values most favorably matched the

Fig. 1. Backbone structure of *Pyrococcus furiosus* rubredoxin indicating residues bearing amide nitrogens within 12 Å of the metal site.

log ratio of the base-catalyzed exchange rate constants for an effective internal dielectric of 6 [31]. In Fig. 2 are illustrated the amide nitrogen differential pK values for the Zn(II) and Ga(III)-forms of *Pf* rubredoxin as deduced from the experimental $\Delta(\log k_{ex})$ values, assuming a purely electrostatic stabilization effect on the peptide anion. These experimental ΔpK values are compared to those predicted by Poisson–Boltzmann calculations for internal dielectric values of 4.5, 6 and 10. Particularly for amide nitrogens with predicted metal charge-dependent differential potentials above 2 kT/e, the ΔpK values estimated from the Poisson–Boltzmann calculations are acutely sensitive to the assumed value for the internal dielectric.

Except for the amides of the charged residues Lys 7 and Glu 48, all differential hydrogen exchange values are predicted to within a $\Delta\Delta pK$ of 0.7 for Poisson–Boltzmann calculations assuming an ε_{int} value of 6. In contrast, under the assumption of an internal dielectric value of 4.5, the Poisson–Boltzmann calculations predict differential amide nitrogen acidities at least 0.7 units greater than those inferred from the hydrogen exchange measurements for five of the other metal charge-dependent residues. Similarly, with an ε_{int} value of 10, five of this set of amides have predicted differential amide nitrogen acidities that are at least 0.7 units less than those estimated from hydrogen exchange. The modest dispersion of the $\Delta\Delta pK$ values predicted by an internal dielectric of 6 compares quite favorably to those for previous studies of strongly shifted sidechain pK values from multiple proteins fitted to a single internal dielectric constant in which the standard deviation of the ΔpK values are approximately one pH unit [6,10,32]. It should be noted in this regard that the differential analysis of the present study does not depend upon referencing to an absolute pK value for the individual amide nitrogens. In contrast, ambiguities regarding the most appropriate reference pK values [14] contribute to the dispersion seen among studies predicting sidechain ionization behavior.

Lys 7 and Glu 48 are the only amides of *Pf* rubredoxin within 11 Å of the metal that bear conformationally mobile charged sidechains. The more strongly positive $\Delta\Delta pK$ values for these two amides are consistent with the argument that the mobile charged sidechains of such residues provide the primary source of enhanced dielectric shielding within proteins [33]. Thirty five (out of 48 non-proline) backbone amides of Zn(II)-substituted *Pf* rubredoxin exchange with bulk solvent sufficiently slowly so as to be detected in these experiments. This set of exchange-protected amides provide an approximate relative volume estimate indicating that roughly 1/3 of the protein interior exhibits metal charge-dependent nitrogen pK values, and all of the corresponding amides appear consistent with effective ε_{int} values near 6.

The consistency between these hydrogen exchange data and the predicted differential amide nitrogen pK values reinforce the inference from the independently determined stability estimates [29] that the change in conformational stability of *Pf* rubredoxin resulting from variation in the metal charge does not substantially contribute to the differential exchange rates used to analyze the electrostatic interactions. More strikingly, the ability to faithfully model these differential hydrogen exchange rates strongly indicates that the transient conformations from which exchange occurs must be closely similar to the native state conformation utilized in the electrostatic analysis [27]. If the distance between each amide nitrogen and the metal site substantially changes in going from the native state to the exchange-competent conformation, the observed correlation with the distances of the X-ray structure would be lost. Furthermore, any larger scale conformational transition to the exchange-competent state would generally increase the amide-metal distances which in turn would yield increased dielectric shielding from the resultant intervening solvent, thus predicting a far weaker electrostatic interaction than is observed.

3.2. Lifetime of buried protein ionizable charges

This analysis of the metal charge-dependent hydrogen exchange for *Pf* rubredoxin indicates effective dielectric shielding that is appreciably less than that often inferred from similar electrostatic calculations that have modeled ionization data for structurally buried sidechains. A potential explanation may lie in the differing lifetimes of the charged states being monitored. All heavy atom reorganization in the protein and in the aqueous/ionic solute environment that occurs on a longer timeframe than the lifetime of a charged intermediate cannot contribute to the effective dielectric shielding of that charged

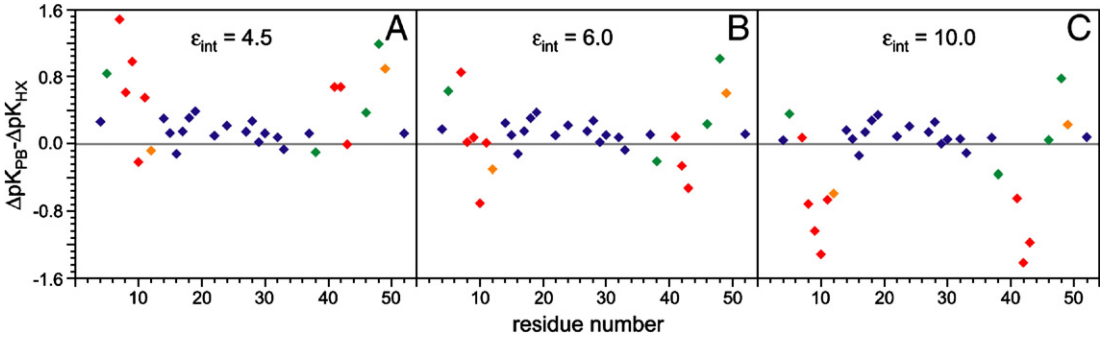

Fig. 2. Deviations between the Poisson–Boltzmann-estimated and hydrogen exchange-derived $\Delta\Delta pK$ values for the nitrogens along the peptide backbone of Zn(II)-substituted vs. Ga(III)-substituted *Pf* rubredoxins. The log ratio of the hydrogen exchange rates ($\Delta\log k_{ex}$) was interpreted to arise from a corresponding metal charge-dependent shift in the pK values of the backbone amide nitrogens. The DelPhi program [17] was used to calculate the electrostatic potential at the nitrogen atoms assuming internal dielectric constant values of 4.5 (A), 6 (B) and 10 (C). The data are color coded according to the metal charge-dependent differential potentials predicted for an ε_{int} of 6 (4–8 kT/e in red, 2–4 kT/e in orange, 1–2 kT/e in green, and <1 kT/e in blue).

state. Although the lifetime of the charged state for the ionizable protein sidechains can be expected to be long when compared to the dielectric relaxation processes that occur in solution, this is not the case for the peptide anion.

In general, *O*-bound and *N*-bound hydrogens act as "normal" acids in the Eigen formalism of acid–base kinetics [34] so that the rate of proton transfer is directly predicted by the differences in p*K*. Hydroxide and hydronium ions react with the neutral carboxylic and amine sidechains at diffusion-limited rates ($k \sim 10^{10}$ M^{-1} s^{-1}). As a result, at pH 7 where $[H^+]$ and $[OH^-]$ are 10^{-7} M, the formation of the charged sidechains occur in approximately a millisecond. When the p*K* value of the ionizable sidechain is close to neutrality, the reverse reaction must likewise occur at a similar rate. Illustration of the experimental determination of these proton transfer rates is provided by the much-studied histidine of the serine protease catalytic triad for which NMR line shape analysis demonstrated that the positively charged imidazolium ring of the α-lytic protease donates a proton to a neutral water molecule at a rate of 3.4×10^3 s^{-1} at 33 °C [35].

The relative rates of the proton transfer reaction between amides and water are reversed from those of ionizable sidechains. Since the neutral amide is a weaker acid than water while the peptide anion is a stronger base than hydroxide (Fig. 3), the hydroxide ion does not react with the amide at a diffusion-limited rate. The ~10 s^{-1} rate for hydroxide-catalyzed exchange of a simple model peptide at pH 7 [36] is a hundred-fold slower than the diffusion controlled, indicating that only approximately one percent of the collisions between hydroxide and a neutral amide results in a proton transfer. Conversely, nearly every collision between a peptide anion and a water molecule will yield a proton transfer reaction. Given the 55 M concentration of water, this diffusion-limited reaction is predicted to occur in a few picoseconds. Although the proton transfer rate to a peptide anion is not easily measured directly, photoactivation of aromatic compounds has proven highly useful in the monitoring of proton transfer kinetics for acidic hydroxyls and ring nitrogen bases [37,38]. Proton transfer times between water and photoactivated strong acids/bases have been observed to be on the order of 10 ps [39,40]. As this range of lifetimes corresponds closely with the $(8\ ps)^{-1}$ rate for the dominant Debye dielectric relaxation mode in bulk phase water [41], solvent reorganization has been proposed to be rate-limiting for the proton transfer reaction between strong acids or bases and water [38]. A similar conclusion is drawn from ^{17}O NMR relaxation measurements [42] which demonstrate that the residence lifetime of an hydroxide ion in water is ~5 ps.

If the lifetime of the peptide anion within the protein interior is similar to its lifetime in solution, the dielectric relaxation behavior of the protein may prove analogous to that observed in the photosynthetic reaction center [43]. Electron transfer from the bacteriochlorophyll special pair to the bacteriopheophytin, and subsequently to the quinone Q_A, occurs in 3 ps [44] and in ~200 ps [45,46], respectively. An effective dielectric value between 4 and 5 has been reported for the latter transition [47], similar to that deduced in the present study. The timeframe of this more slowly relaxing phase of the photosynthetic reaction center may be compared to molecular dynamics studies which have argued that a substantial proportion of the dielectric relaxation in a protein occurs in the range of a few hundred picoseconds [48] to several nanoseconds [49].

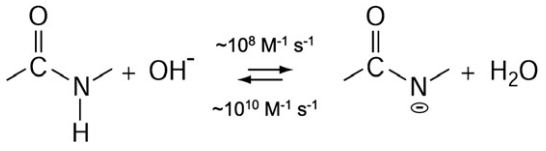

Fig. 3. Hydroxide ion-catalyzed exchange of the amide hydrogen. The pK_a of the amide nitrogen is approximately two units higher than that of water. The peptide anion reacts with the neutral water molecule at a diffusion-limited rate, while the reverse reaction has a hundred-fold smaller rate constant.

In general, burial of an ionizable group without a compensatory counter-charge leads to a suppression of ionization and a corresponding change in the observed p*K* value. Two limiting paradigms can be used to characterize the subsequent process for the long-lived charged state of an ionizable sidechain. In one case, the native structure cannot stabilize the charged sidechain so that this group must become exposed to solvent before becoming ionized. That ionization then "traps" the protein in this solvent-exposed state until a subsequent proton transfer regenerates the neutral sidechain and refolding to the native state can occur. Under this condition, the observed shift in p*K* will primarily reflect the free energy cost of generating the solvent-exposed conformation.

In the opposite limiting case, the ionized sidechain can be accommodated within the protein interior. Transient solvent access to this ionized sidechain will eventually lead to the proton transfer needed to return to the neutral sidechain state. If the relative time of the conformational transition leading to solvent access is short compared to the overall lifetime of the buried charged state, the observed p*K* and the apparent dielectric constant will reflect the shielding properties of the protein in the neutral sidechain conformation combined with the dielectric relaxation response arising from the charging of the sidechain group. On the other hand, the kinetics and free energy of the transient conformational transition that gives rise to the proton transfer will not be reflected in either the p*K* or the apparent dielectric constant.

The extensively studied staphylococcal nuclease system offers insight into the structural response of a protein to the presence of a buried charged sidechain. Although crystal structures of the neutral sidechain forms for the V66E [50], V66K [51] and V66D [52] variants have been reported, no such structures are available for the less stable charged states of these proteins. Although fluorescence and circular dichroism measurements have not detected any structural changes occurring upon ionization of either the glutamic acid or lysine sidechains, there is evidence for a loss of up to 1 1/2 turns of α-helix for the aspartic acid variant [52]. With the availability of X-ray structures for the neutral sidechain states, nearly all electrostatic analyses of these staphylococcal nuclease ionizations have utilized a buried charged sidechain model. However, utilizing an "overcharging" approach to accelerate the conformation transition via molecular dynamics simulation, the modeling of the ionization-induced partial unfolding of the staphylococcal nuclease V66E variant has recently been reported [53].

The comparatively short lifetime of the peptide anion implies significant kinetic differences in the protein structural response to formation of the charged state. As nearly every collision between a peptide anion and a neutral water molecule will lead to a proton transfer, the analogous trapping of this peptide in a locally unfolded solvent-exposed conformational state cannot occur. Similarly, given that both hydronium and hydroxide equivalents diffuse through water significantly faster than do the oxygen atoms [54], the lifetime of a structurally buried peptide anion can be expected to be short as compared to the diffusion of water in and out of the protein interior. Hence, the same transient conformational process which provides the solvent access that leads to the generation of the peptide anion will generally also serve to quench that anion back to the neutral state before returning to the solvent-inaccessible state. Since the solvation which leads to proton transfer will generally be present throughout the lifetime of the buried peptide anion, that solvated state will contribute directly to the resultant dielectric relaxation.

4. Conclusions

In the analysis of the conformationally dependent p*K* shifts that arise for the weak acids and bases of the amino acid sidechains, a static dielectric constant is generally implicitly assumed. Given the long lifetimes of both the neutral and charged states for these groups, the assumption that the dielectric shielding of the system becomes completely relaxed is generally well justified. However, when the lifetime of a transient charged state becomes comparable to the timeframe over which the structural response occurs, the dynamic dependence of dielectric shielding must be considered. The time dependence of heavy atom reorganization is well known to be central to the analysis of electron transfer studies [55]. However, the frequency dependence of dielectric shielding is less often invoked in other aspects of protein chemistry. Stabilization of the nearly ubiquitous occurrence of transient charged intermediate states in enzymatic reactions reflects these effects [56–58]. The hydrogen exchange of rubredoxin offers a system in which a number of such transient charged intermediates are generated in parallel. The limited differences in conformational stability for the various metal charge states warrants interpreting the differential exchange rates in terms of dielectric shielding effects. The lifetimes of these peptide anions are short compared to the practical length of unconstrained molecular dynamics simulations. As a result, detailed analysis of the dielectric shielding in these reactions may prove feasible.

Acknowledgments

This work was supported in part by NIH grant GM 64736 (G.H.).

References

[1] C. Tanford, J.G. Kirkwood, Theory of protein titration curves. I. General equations for impenetrable spheres, J. Am. Chem. Soc. 79 (1957) 5333–5339.
[2] J.C. Kendrew, G. Bodo, H.M. Dintzis, R.G. Parrish, H. Wyckoff, D.C. Phillips, A three-dimensional model of the myoglobin molecule obtained by X-ray analysis, Nature 181 (1958) 662–666.
[3] S. Hofinger, T. Simonson, Dielectric relaxation in proteins: a continuum electrostatics model incorporating dielectric heterogeneity of the protein and time-dependent charges, J. Comput. Chem. 22 (2001) 290–305.
[4] T. Simonson, J. Carlsson, D.A. Case, Proton binding to proteins: pKa calculations with explicit and implicit solvent models, J. Am. Chem. Soc. 126 (2004) 4167–4180.
[5] M. Kato, A.V. Pisliakov, A. Warshel, The barrier for proton transport in aquaporins as a challenge for electrostatic models: the role of protein relaxation in mutational calculations, Proteins 64 (2006) 829–844.
[6] C.N. Schutz, A. Warshel, What are the dielectric "constants" of proteins and how to validate electrostatic models, Proteins. Struct. Funct. Bioinform. 44 (2001) 400–417.
[7] H. Li, A.D. Robertson, J.H. Jensen, Very fast empirical prediction and rationalization of protein pKa values, Proteins. Struct. Funct. Bioinform. 61 (2005) 704–721.
[8] J. Antosiewicz, J. McCammon, M. Gilson, Prediction of pH dependent properties of proteins, J. Mol. Biol. 238 (1994) 415–436.
[9] K. Langsetmo, J.A. Fuchs, C. Woodward, K.A. Sharp, Linkage of thioredoxin stability to titration of ionizable groups with perturbed pKa, Biochemistry 30 (1991) 7609–7614.
[10] E. Demchuk, R. Wade, Improving the continuum dielectric approach to calculating pKa's of ionizable groups in proteins, J. Phys. Chem. 100 (1996) 17373–17387.
[11] B. Garcia-Moreno, J.J. Dwyer, A.G. Gittis, E.E. Lattman, D.S. Spencer, W.E. Stites, Experimental measurement of the effective dielectric in the hydrophobic core of a protein, Biophys. Chemist. 64 (1997) 211–224.
[12] M.F. García-Mayoral, J.M. Pérez-Cañadillas, J. Santoro, B. Ibarra-Molero, J.M. Sanchez-Ruiz, J. Lacadena, A.M.D. Pozo, J.G. Gavilanes, M. Rico, M. Bruix, Dissecting structural and electrostatic interactions of charged groups in a-sarcin. An NMR study of some mutants involving the catalytic residues, Biochemistry 42 (2003) 13122–13133.
[13] D.V. Laurents, B.M.P. Huyghues-Despointes, M. Bruix, R.L. Thurkill, D. Schell, S. Newsom, G.R. Grimsley, K.L. Shaw, S. Treviño, M. Rico, J.M. Briggs, J.M. Antosiewicz, J.M. Scholtz, C.N. Pace, Charge–charge interactions are key determinants of the p*K* values of ionizable groups in ribonuclease Sa (p*I*=3.5) and a basic variant (p*I*=10.2), J. Mol. Biol. 325 (2003) 1077–1092.
[14] R.L. Thurkill, G.R. Grimsley, J.M. Scholtz, C.N. Pace, p*K* values of the ionizable groups of proteins, Protein Sci. 15 (2006) 1214–1218.
[15] R. Bau, D.C. Rees, D.M. Kurtz, R.A. Scott, H.S. Huang, M.W.W. Adams, M.K. Eidsness, Crystal-structure of rubredoxin from *Pyrococcus furiosus* at 0.95 Å resolution, and the structures of N-terminal methionine and formylmethionine variants of *Pf* Rd. Contributions of N-terminal interactions to thermostability, J. Biol. Inorg. Chem. 3 (1998) 484–493.
[16] J.M. Word, S.C. Lovell, J.S. Richardson, D.C. Richardson, Asparagine and glutamine: using hydrogen atom contacts in the choice of side-chain amide orientation, J. Mol. Biol. 285 (1999) 1733–1747.
[17] W. Rocchia, S. Sridharan, A. Nicholls, E. Alexov, A. Chiabrera, B. Honig, Rapid grid-based construction of the molecular surface and the use of induced surface charge to calculate reaction field energies: applications to the molecular systems and geometric objects, J. Comput. Chem. 23 (2002) 128–137.
[18] D. Sitkoff, K.A. Sharp, B. Honig, Accurate calculation of hydration free energies using macroscopic solvent models, J. Phys. Chem. 98 (1994) 1978–1988.
[19] J.B. Koerner, T. Ichiye, Conformational dependence of the electronic properties of $[Fe(SCH3)4]^{-,2-}$, J. Phys. Chem., B 101 (1997) 3633–3643.
[20] B.W. Beck, J.B. Koerner, T. Ichiye, Ab initio quantum mechanical study of metal substitution in analogues of rubredoxin: implications for redox potential control, J. Phys. Chem., B 103 (1999) 8006–8015.
[21] Z. Dauter, K.S. Wilson, L.C. Sieker, J.M. Moulis, J. Meyer, Zinc- and iron-rubredoxins from *Clostridium pasteurianum* at atomic resolution: a high precision model of a ZnS4 coordination unit in a protein, Proc. Natl. Acad. Sci. U. S. A. 93 (1996) 8836–8840.
[22] T.P. Min, C.E. Ergenekan, M.K. Eidsness, T. Ichiye, C.H. Kang, Leucine 41 is a gate for water entry in the reduction of *Clostridium pasteurianum* rubredoxin, Protein Sci. 10 (2001) 613–621.

[23] M. Maher, M. Cross, M.C.J. Wilce, J.M. Guss, A.G. Wedd, Metal-substituted derivatives of the rubredoxin from *Clostridium pasteurianum*, Acta Crystallogr., D Biol. Crystallogr. 60 (2004) 298–303.
[24] K.D. Watenpaugh, L.C. Sieker, L.H. Jensen, The structure of rubredoxin at 1.2 Å resolution, J. Mol. Biol. 131 (1979) 509–522.
[25] G. Hernández, C.L. Teng, R.G. Bryant, D.M. LeMaster, O2 penetration and proton burial depth in proteins: applicability to fold family recognition, J. Am. Chem. Soc. 124 (2002) 4463–4472.
[26] J. Tang, G. Hernández, D.M. LeMaster, Increased peptide deformylase activity for the *N*-formylmethionine processing of proteins overexpressed in *Escherichia coli*: application to homogeneous rubredoxin production, Protein Expr. Purif. 36 (2004) 100–105.
[27] D.M. LeMaster, J.S. Anderson, G. Hernández, Role of native-state structure in rubredoxin native-state hydrogen exchange, Biochemistry 45 (2006) 9956–9963.
[28] R. Hiller, Z.H. Zhou, M.W.W. Adams, S.W. Englander, Stability and dynamics in a hyperthermophilic protein with melting temperature close to 200 °C, Proc. Natl. Acad. Sci. U. S. A. 94 (1997) 11329–11332.
[29] W.Y. Sun, N. Ueyama, A. Nakamura, Electrochemical mimicking of reduced rubredoxin by iron(II) complexes of cysteine peptide thiolate in aqueous micelle solution, J. Electroanal. Chem. 448 (1998) 105–109.
[30] J.W.R. Schwabe, A. Klug, Zinc mining for protein domains, Nat. Struct. Biol. 1 (1994) 345–349.
[31] J.S. Anderson, D.M. LeMaster, G. Hernandez, Electrostatic potential energy within a protein monitored by metal charge-dependent hydrogen exchange, Biophys. J. 91 (2006) L93–L95.
[32] D. Bashford, Macroscopic electrostatic models for protonation states in proteins, Front. Biosci. 9 (2004) 1082–1099.
[33] T. Simonson, D. Perahia, Internal and interfacial dielectric properties of cytochrome *c* from molecular dynamics in aqueous solution, Proc. Natl. Acad. Sci. U. S. A. 92 (1995) 1082–1086.
[34] M. Eigen, Proton transfer, acid-base catalysis, and enzymic hydrolysis. (I) Elementary processes, Angew. Chem., Int. Ed. Engl. 3 (1964) 1–72.
[35] E.L. Ash, J.L. Sudmeier, R.M. Day, M. Vincent, E.V. Torchilin, K.C. Haddad, E.M. Bradshaw, D.G. Sanford, W.W. Bachovchin, Unusual 1H NMR chemical shifts support (His) Ce1–H…O═C H-bond: proposal for reaction-driven ring flip mechanism in serine protease catalysis, Proc. Natl. Acad. Sci. U. S. A. 97 (2000) 10371–10376.
[36] R.S. Molday, R.G. Kallen, Substituent effects on amide hydrogen exchange rates in aqueous solution, J. Am. Chem. Soc. 94 (1972) 6739–6745.
[37] J.F. Ireland, P.A.H. Wyatt, Acid–base properties of electronically excited states of organic molecules, Adv. Phys. Org. Chem. 12 (1976) 131–160.
[38] L.M. Tolbert, K.M. Solntsev, Excited-state proton transfer: from constrained systems to "super" photoacids to superfast proton transfer, Acc. Chem. Res. 35 (2002) 19–27.
[39] P. Leiderman, L. Genosar, D. Huppert, Excited-state proton transfer: indication of three steps in the dissociation and recombination process, J. Phys. Chem., A 109 (2005) 5965–5977.
[40] H.J. Park, O.H. Kwon, C.S. Ah, D.J. Jang, Excited-state tautomerization dynamics of 7-hydroxyquinoline in b-cyclodextrin, J. Phys. Chem., B 109 (2005) 3938–3943.
[41] W.J. Ellison, K. Lamkaouchi, J.M. Moreau, Water: a dielectric reference, J. Mol. Liq. 68 (1996) 171–279.
[42] Z. Luz, S. Meiboom, The activation energies of protein transfer reactions in water, J. Am. Chem. Soc. 86 (1964) 4768–4769.
[43] C.C. Moser, C.C. Page, R.J. Cogdell, J. Barber, C.A. Wraight, P.L. Dutton, Length, time and energy scales of photosystems, Adv. Protein Chem. 63 (2003) 71–109.
[44] J. Breton, J.L. Martin, A. Migus, A. Antonetti, A. Orzag, Femtosecond spectroscopy of excition energy transfer and initial charge separation in the reaction center of the photosynthetic bacterium *Rhodopseudomonas viridis*, Proc. Natl. Acad. Sci. U. S. A. 83 (1986) 5121–5125.
[45] K.J. Kaufmann, P.L. Dutton, T.L. Netzel, J.S. Leigh, Rentzepis, picosecond kinetics of events leading to reaction center bacteriochlorophyll oxidation, Science 188 (1975) 1301–1305.
[46] M.G. Rockley, M.W. Windsor, R.J. Cogdell, W.W. Parson, Picosecond detection of an intermediate in the photochemical reaction of bacterial photosynthesis, Proc. Natl. Acad. Sci. U. S. A. 72 (1975) 2251–2255.
[47] M.A. Steffen, K. Lao, S.G. Boxer, Dielectric asymmetry in the photosynthetic reaction center, Science 264 (1994) 810–816.
[48] B.N. Dominy, H. Minoux, C.L.B. III, An electrostatic basis for the stability of thermophilic proteins, Proteins 57 (2004) 128–141.
[49] P.E. Smith, R.M. Brunne, A.E. Mark, W.F. vanGunsteren, Dielectric properties of trypsin inhibitor and lysozyme calculated from molecular dynamics, J. Phys. Chem. 97 (1993) 2009–2014.
[50] J.J. Dwer, A.G. Gittis, D.A. Karp, E.E. Lattman, D.S. Spencer, W.E. Stites, E.B. Garcia-Moreno, High apparent dielectric constants in the interior of a protein reflect water penetration, Biophys. J. 79 (2000) 1610–1620.
[51] W.E. Stites, A.G. Gittis, E.E. Lattman, D. Shortle, In a staphylococcal nuclease mutant the sidechain of a lysine replacing valine-66 is fully buried in the hydrophobic core, J. Mol. Biol. 221 (1991) 7–14.
[52] D.A. Karp, A.G. Gittis, M.R. Stahley, C.A. Fitch, W.E. Stites, B.E. García-Moreno, High apparent dielectric constant inside a protein reflects structural reorganization coupled to the ionization of an internal Asp, Biophys. J. 92 (2007) 2041–2053.
[53] M. Kato, A. Warshel, Using a charging coordinate in studies of ionization induced partial unfolding, J. Phys. Chem., B 110 (2006) 11566–11570.
[54] M.E. Tuckerman, A. Chandra, D. Marx, Structure and dynamics of OH^- (aq), Acc. Chem. Res. 39 (2006) 151–158.
[55] H.B. Gray, J.R. Winkler, Electron transfer in proteins, Ann. Rev. Biochem. 65 (1996) 537–561.
[56] T. Simonson, G. Archontis, M. Karplus, A Poisson–Boltzmann study of charge interactions in an enzyme active site: the effect of dielectric relaxation, J. Phys. Chem., B 103 (1999) 6142–6156.
[57] E.L. Mertz, L.I. Krishtalik, Low dielectric response in enzyme active site, Proc. Natl. Acad. Sci. U. S. A. 97 (2000) 2081–2086.
[58] G. Archontis, T. Simonson, Dielectric relaxation in an enzyme active site: molecular dynamics simulations interpreted with a macromolecular continuum model, J. Am. Chem. Soc. 123 (2001) 11047–11056.